Chalcogenide Letters Vol. 21, No.8, August 2024, p. 651 - 663

Improvement and optimization of $Cu_2ZnSn(S_{1-x}Se_x)_4$ structure for optoelectronic applications

A. Skender[a], A. Aissat [a,b,c,*], J. P. Vilcot[c]
[a]*LATSI Laboratory, Faculty of Technology, University of Saad Dahlab Blida1, Algeria*
[b]*University of Ahmed Draia, Adrar, Algeria*
[c]*Institute of Electronics, Microelectronics and Nanotechnology (IEMN), UMR CNRS 8520, University of Sciences and Technologies of Lille 1, Avenue Poincare, 60069, 59652 Villeneuve of Ascq, France*

The use of semiconductors based on abundant and less expensive materials in photovoltaic industry has grown since electricity consumption has increased, alloys such as $Cu_2ZnSn(S_{1-x}Se_x)_4$ have recently attracted attention, due to its structural, optical and electronic properties which make it a very promising candidate as an absorber layer in photovoltaic applications. The lattice mismatch of $Cu_2ZnSn(S_{1-x}Se_x)_4$ with Cu_2NiGeS_4 as substrate for solar cell architecture reveals that low *Se* content ($0.1 \leq x \leq 0.4$) is favorable, and thus, by reducing *Se* content from 40 to 10% induces a decrease in optical parameters such as refractive index from 5.475 to 3.834 for near-infrared wavelengths, and both extinction and absorption coefficients are from 0.478 to 0.211 and from 7.956×10^4 to 6.912×10^4 cm^{-1}, respectively, for almost along the visible spectrum. Additionally, the bandgap energy of $Cu_2ZnSn(S_{1-x}Se_x)_4$ in kesterite structure increases from 1.267 to 1.442 eV at room temperature, while the compressive strain of the epitaxial layer reduces from 3.93 to 2.39% and from 4.62 to 3.17% on the growth plane and following the direction of growth, respectively.

(Received May 18, 2024; August 15, 2024)

Keywords: Materials, Semiconductors, Thin films, Solar cell, Photovoltaic, Optoelectronics

1. Introduction

Despite the advantage brought by $Cu(In_{1-x}Ga_x)Se_2$ (*CIGS*) solar cells in terms of efficiency, they have other disadvantages, mainly due to the fact that indium and gallium resources are limited, rare and expensive, which pushed researchers to use other materials. $Cu_2ZnSn(S_{1-x}Se_x)_4$ (*CZTSSe*) kesterites based devices have attracted attention, since these absorbers are potential substitutes for $Cu(In_{1-x}Ga_x)Se_2$ (*CIGS*) in photovoltaic applications.Wang *et al*. reported that a *CZTSSe* based solar cell in kesterite structure provided a conversion efficiency of 12.6% [1].

According to Shen *et al*. sequential cation cross-substitution can be used to obtain *CZTSe* in kesterite structure from zinc blende through an intermediate chalcopyrite structure[2][3]. Li *et al*. reported that for *CdTe* in zinc blende structure, the cation *Cd* and the anion *Te* are located independently in two face-centered cubic lattices which are interpenetrated, and thus, the doubling of the unit cell along the c axis allows us to obtain the chalcopyrite $CuInSe_2$ from the zinc blende structure by substituting on the one hand *Cd* by ordered *Cu* and *In* and on the other hand *Te* by *Se*, then, replacing *In* by ordered *Zn* and *Sn* allows us to obtain kesterite $Cu_2ZnSnSe_4$ [4].Taking into account that in structure derivation process, the anion atoms occupy one face-centered cubic lattice and the cation atoms occupy the other one [4].

Moreover, according to a new and easy method developed in reference [5], Shi *et al*. report that *CZTSSe* crystal growth can be achieved by air annealing of a *CZTS* thin film, followed by *Na* diffusion with surface oxidation, thereby considerably promoting the growth of *CZTSSe* absorber layer and eliminates the small grains of the bottom layer.

*Corresponding author: sakre23@yahoo.fr
https://doi.org/10.15251/CL.2024.218.651

Two types of crystal structures (kesterite and stannite) are known for *CZTS* and *CZTSe* semiconductor materials, which they have been studied experimentally in references [6] and [7] and theoretically in references [8] and [9]. From the point of view of phase stability, Kumar *et al.* report that kesterite structure is more stable than stannite structure [10].

On the other hand, Persson reported that the crystallization of *CZTS* and *CZTSSe* materials in both kesterite and stannite structures can be verified from a large difference between their dielectric functions [11].

The aim of this work is to determine the different structural, optical and electronic properties of *CZTSSe* which can ensure its usefulness in optoelectronics as well as in photovoltaic applications as an absorber layer for a simple or multi-junction solar cell.

2. Theoretical model

Knowing that the properties of a semiconductor material strongly depend on the concentration of its compounds, it is necessary to take this characteristic into consideration to better extract good results with regard to the performance of this material, in $Cu_2ZnSn(S_{1-x}Se_x)_4$ alloys, the Se content allowing to acquire certain advantages.

Since epitaxially grown heterostructures now commonly combine layers of mismatched lattice constituents, the properties of a material under stress must also be specified, this is classically done in strain potential theory [12].

When a structure is developed from two materials whose lattice parameters are different, a phenomenon of epitaxial deformation will take place on the growth plane and following the growth direction (relation (1) and (2), respectively) due to the formation of a coherent interface between the two materials, which results a different lattice parameter from those of the precedent two materials [3].

$$\boldsymbol{\varepsilon_{xx} = \varepsilon_{yy} = \frac{a_s - a_e}{a_e}} \quad (1)$$

$$\varepsilon_{zz} = \frac{c_s - c_e}{c_e} = -\frac{c_{12}}{c_{11}}\varepsilon_{xx} \quad (2)$$

Where a_s and c_s are the lattice parameters of the substrate, a_e and c_e are the lattice parameters of the epitaxial layer, C_{11} and C_{12} are elasticity constants. Fig.1. shows the growth of $Cu_2ZnSn(S_{1-x}Se_x)_4$ on Cu_2NiGeS_4 substrate.

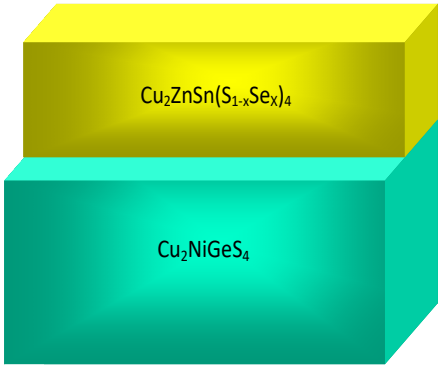

Fig.1.Growth of $Cu_2ZnSn(S_{1-x}Se_x)_4$ on Cu_2NiGeS_4 substrate.

Table 1. Lattice parameters of Cu_2ZnSnS_4 and $Cu_2ZnSnSe_4$ in kesterite and stannite structures with Cu_2NiGeS_4 in stannite structure.

	Cu_2ZnSnS_4 [10]		$Cu_2ZnSnSe_4$ [10]		Cu_2NiGeS_4 [13]
	Kesterite	Stannite	Kesterite	Stannite	Stannite
a(Å)	5.440	5.450	5.732	5.738	5.338
c(Å)	10.864	10.878	11.418	11.454	10.573

The interface structure in multilayers can be predicted from the forces on the dislocation lines. Two of the important forces are the force exerted by the maladaptive deformation and the tension in the dislocation line [15]. Among the criteria which must be taken into account in thin film production processes, it is necessary to avoid the formation of recombination centers that come from dislocation at the active interface, this interface must be perfectly in good crystalline quality, for this reason, the thickness of the epitaxial layer is limited by a value called critical thickness h_c which it must not exceed to ensure an excellent heteroepitaxial growth [14].

$$\boldsymbol{h_c = \frac{a_e(1-0.25\gamma)}{k\sqrt{2}\pi\varepsilon_{xx}(1+\gamma)} ln\left(\frac{h_c}{a_e}\sqrt{2}+1\right)} \quad (3)$$

Where k is a coefficient which takes the values of 1, 2 or 4 for a superlattice, a quantum well or a single layer, respectively, and γ is the Poisson's coefficient:

$$\boldsymbol{\gamma = \frac{C_{12}(x)}{C_{11}(x)+C(x)}} \quad (4)$$

With $C_{11}(x)$ and $C_{12}(x)$ are the elastic constants.

On the other hand, the dielectric constant depends on the wavelength λ and it can be calculated by the first order Sellmeier equation (6) [19], where its parameters are mentioned in table.2. For $Cu_2ZnSn(S_{1-x}Se_x)_4$ alloys, the dielectric constant can be anticipated from the modified Vegard's law:

$$\varepsilon_1^{Cu_2ZnSn(S_{1-x}Se_x)_4}(x) = \varepsilon_1^{Cu_2ZnSnS_4}(1-x) + \varepsilon_1^{Cu_2ZnSnSe_4}x - b_{\varepsilon_1}^{Cu_2ZnSn(S_{1-x}Se_x)_4}x(1-x) \quad (5)$$

Where $\varepsilon_1^{Cu_2ZnSnS_4}$ and $\varepsilon_1^{Cu_2ZnSnSe_4}$ are the dielectric constants of Cu_2ZnSnS_4 and $Cu_2ZnSnSe_4$, materials respectively, $b_{\varepsilon_1}^{Cu_2ZnSn(S_{1-x}Se_x)_4}$ =-0.221 is the bowing parameter of $Cu_2ZnSn(S_{1-x}Se_x)_4$ dielectric constant [22].

Additionally, Li *et al*. used the spectroscopic ellipsometry to study the optical constants of *CZTS* [18], as it has been applied on certain Cu_2-*II-IV-VI*$_4$ semiconductors for a fairly wide spectral range [19], on Cu_2ZnGeS_4[16] and on *CZTSe* [17]. Therefore, the first order Sellmeier equation makes it possible to obtain the refractive indices of semiconductors by extrapolation of their data resulting from spectroscopic ellipsometry [19]:

$$n^2(\lambda) = \varepsilon_1(\lambda) = A + \frac{B\lambda^2}{\lambda^2 - C^2} \quad (6)$$

Where A, B and C are the fitting parameters, their values are mentioned in table.3, and λ is the wavelength. The refractive index $\boldsymbol{n_{Cu_2ZnSn(S_{1-x}Se_x)_4}(x,\lambda)}$ of $Cu_2ZnSn(S_{1-x}Se_x)_4$ semiconductor depends on the *Se* content, and it can be determined by the modified Vegard's law:

$$\boldsymbol{n_{Cu_2ZnSn(S_{1-x}Se_x)_4}(x,\lambda) = n_{Cu_2ZnSnS_4}(\lambda)(1-x) + n_{Cu_2ZnSnSe_4}(\lambda)x - b_n^{Cu_2ZnSn(S_{1-x}Se_x)_4}x(1-x)} \quad (7)$$

Where $\boldsymbol{n_{Cu_2ZnSnS_4}(\lambda)}$ and $\boldsymbol{n_{Cu_2ZnSnSe_4}(\lambda)}$, are the refractive indices of Cu_2ZnSnS_4 and $Cu_2ZnSnSe_4$, respectively, $\boldsymbol{b_n^{Cu_2ZnSn(S_{1-x}Se_x)_4}}$ is the bowing parameter of $Cu_2ZnSn(S_{1-x}Se_x)_4$ refractive index.

Table 2. Fitting parameters A, B and C of Sellmeier equation of the refractive index n for Cu_2ZnSnS_4 and $Cu_2ZnSnSe_4$with the bowing parameter of $Cu_2ZnSn(S_{1-x}Se_x)_4$ refractive index.

	Cu_2ZnSnS_4 [20]	$Cu_2ZnSnSe_4$ [20]
A	3.10	6.80
B	3.85	2.30
C^2(μm^2)	0.220	0.660
	$Cu_2ZnSn(S_{1-x}Se_x)_4$ [21]	
b_n	-0.058	

Moreover, the effectiveness of a material in absorbing light of a particular wavelength is indicated by the extinction coefficient *k* [23], which can be estimated using the equation:

$$k_{Cu_2ZnSn(S_{1-x}Se_x)_4}(x,\lambda) = \frac{\lambda\alpha_{Cu_2ZnSn(S_{1-x}Se_x)_4}(x,\lambda)}{4\pi} \quad (8)$$

Where $\boldsymbol{k_{Cu_2ZnSn(S_{1-x}Se_x)_4}(x,\lambda)}$is the extinction coefficient and $\boldsymbol{\alpha_{Cu_2ZnSn(S_{1-x}Se_x)_4}}$is the absorption coefficient of $Cu_2ZnSn(S_{1-x}Se_x)_4$.

Moreover, the bandgap energy of Cu_2ZnSnS_4 and $Cu_2ZnSnSe_4$ in the kesterite crystal structure derived from zinc blende structure are very well consistent with the experimental measurement [24].Since the composition of $Cu_2ZnSn(S_{1-x}Se_x)_4$ alloys can be tuned with good miscibility, therefore, their bandgaps depend on *Se* content.

$$\boldsymbol{E_g^{Cu_2ZnSn(S_{1-x}Se_x)_4}(x) = E_g^{Cu_2ZnSnS_4}(1-x) + E_g^{Cu_2ZnSnSe_4}x - b_{E_g}^{Cu_2ZnSn(S_{1-x}Se_x)_4}x(1-x)} \quad (9)$$

Where $\boldsymbol{E_g^{Cu_2ZnSnS_4}}$ and $\boldsymbol{E_g^{Cu_2ZnSnSe_4}}$ are Cu_2ZnSnS_4 and $Cu_2ZnSnSe_4$ bandgaps, respectively, $\boldsymbol{b_{E_g}^{Cu_2ZnSn(S_{1-x}Se_x)_4}}$ is the bowing parameter of $Cu_2ZnSn(S_{1-x}Se_x)_4$ bandgap energy.

Table 3. Cu_2ZnSnS_4 and $Cu_2ZnSnSe_4$ bandgaps with the bowing parameter of $Cu_2ZnSn(S_{1-x}Se_x)_4$bandgap.

	Cu_2ZnSnS_4[21]	$Cu_2ZnSnSe_4$[21]
	Kesterite	
E_g(eV)	1.505	0.984
	$Cu_2ZnSn(S_{1-x}Se_x)_4$[21]	
b_{E_g}(eV)	0.123	

The temperature effect on the evolution of $Cu_2ZnSn(S_{1-x}Se_x)_4$ bandgap energy could be modeled by Varshni relation:

$$\boldsymbol{E_g^{Cu_2ZnSn(S_{1-x}Se_x)_4}(x,T) = E_g^{Cu_2ZnSn(S_{1-x}Se_x)_4}(x,0) - \frac{\alpha_{E_g}^{Cu_2ZnSn(S_{1-x}Se_x)_4}(x)T^2}{\beta_{E_g}^{Cu_2ZnSn(S_{1-x}Se_x)_4}(x)+T}} \quad (10)$$

Where $\boldsymbol{E_g^{Cu_2ZnSn(S_{1-x}Se_x)_4}(x,0)}$ is $Cu_2ZnSn(S_{1-x}Se_x)_4$ bandgap at T =0 K, $\boldsymbol{\alpha_{E_g}^{Cu_2ZnSn(S_{1-x}Se_x)_4}(x)}$ and $\boldsymbol{\beta_{E_g}^{Cu_2ZnSn(S_{1-x}Se_x)_4}(x)}$ are empirical parameters that can be determined by Vegard's law:

$$\boldsymbol{\alpha_{E_g}^{Cu_2ZnSn(S_{1-x}Se_x)_4}(x) = \alpha_{E_g}^{Cu_2ZnSnS_4}(1-x) + \alpha_{E_g}^{Cu_2ZnSnSe_4}x} \quad (11)$$

$$\beta_{E_g}^{Cu_2ZnSn(S_{1-x}Se_x)_4}(x) = \beta_{E_g}^{Cu_2ZnSnS_4}(1-x) + \beta_{E_g}^{Cu_2ZnSnSe_4}x \quad (12)$$

$E_g^{Cu_2ZnSn(S_{1-x}Se_x)_4}(x,0)$ can be calculated by relation (13):

$$E_g^{Cu_2ZnSn(S_{1-x}Se_x)_4}(x,0) = E_g^{Cu_2ZnSnS_4}(0)(1-x) + E_g^{Cu_2ZnSnSe_4}(0)x - b_{E_g}^{Cu_2ZnSn(S_{1-x}Se_x)_4}x(1-x) \quad (13)$$

Where $E_g^{Cu_2ZnSnS_4}(0)$ and $E_g^{Cu_2ZnSnSe_4}(0)$ are the bandgaps of *Cu₂ZnSnS₄* and *Cu₂ZnSnSe₄*, respectively, at $T = 0$ K.

Table 4. Bandgap $E_g(0)$ at T = 0 K and the adjustment parameters α and β of Varshni relation of Cu₂ZnSnS₄ and Cu₂ZnSnSe₄.

	Cu₂ZnSnS₄ [25]	*Cu₂ZnSnSe₄*
$E_g(0)$ (eV)	1.64	1.05[a]
$\alpha_{E_g}\times10^{-4}$(eV.K^{-1})	10.1	1.35[b]
β_{E_g}(K)	340	413[c]

a is the bandgap $E_g(0)$ value of Cu₂ZnSnSe₄ at T = 0 K which is deduced from reference [26].
b and c are respectively the values of the parameters α_{E_g} and β_{E_g} of Cu₂ZnSnSe₄ which are deduced from reference [27].

On the other side, the absorption coefficient can be determined using Tauc model [22]:

$$\boldsymbol{\alpha h\upsilon = \alpha_0\left(h\upsilon - E_g\right)^m \text{ with } h\upsilon > E_g} \quad (14)$$

Where $h\upsilon$ is the energy of the incident photon, h is the Planck constant, υ is the frequency of the incident light, E_g is the energy of the optical bandgap, α_0 is an energy dependent constant and m is an index which depends on the optical transition caused by the absorption of photons, the value of m is 0.5 for direct bandgap semiconductors. Thus, the absorption coefficient as a function of wavelength is written:

$$\alpha_{Cu_2ZnSnS_4}(\lambda) = \alpha_0^{Cu_2ZnSnS_4}\frac{\sqrt{\frac{hc}{\lambda}-E_g^{Cu_2ZnSnS_4}}}{\frac{hc}{\lambda}} \quad (15)$$

$$\alpha_{Cu_2ZnSnSe_4}(\lambda) = \alpha_0^{Cu_2ZnSnSe_4}\frac{\sqrt{\frac{hc}{\lambda}-E_g^{Cu_2ZnSnSe_4}}}{\frac{hc}{\lambda}} \quad (16)$$

Where $\alpha_{Cu_2ZnSnS_4}(\lambda)$ and $\alpha_{Cu_2ZnSnSe_4}(\lambda)$ are the absorption coefficients of *Cu₂ZnSnS₄* and *Cu₂ZnSnSe₄*, respectively, $E_g^{Cu_2ZnSnS_4}$ and $E_g^{Cu_2ZnSnSe_4}$ are their respective bandgaps whose values are mentioned in table.5, $\alpha_0^{Cu_2ZnSnS_4}$ and $\alpha_0^{Cu_2ZnSnSe_4}$ are their respective energy dependent constants.

The absorption coefficient $\boldsymbol{\alpha_{Cu_2ZnSn(S_{1-x}Se_x)_4}(x,\lambda)}$ of $Cu_2ZnSn(S_{1-x}Se_x)_4$ semiconductor also depends on *Se* content:

$$\boldsymbol{\alpha_{Cu_2ZnSn(S_{1-x}Se_x)_4}(x,\lambda) = \alpha_0^{Cu_2ZnSn(S_{1-x}Se_x)_4}(x)\frac{\sqrt{\frac{hc}{\lambda}-E_g^{Cu_2ZnSn(S_{1-x}Se_x)_4}(x)}}{\frac{hc}{\lambda}}} \quad (17)$$

The constant $\boldsymbol{\alpha_0^{Cu_2ZnSn(S_{1-x}Se_x)_4}(x)}$ can be determined by the modified Vegard's law:

$$\boldsymbol{\alpha_0^{Cu_2ZnSn(S_{1-x}Se_x)_4}(x) = \alpha_0^{Cu_2ZnSnS_4}(1-x) + \alpha_0^{Cu_2ZnSnSe_4}x - b_\alpha^{Cu_2ZnSn(S_{1-x}Se_x)_4}x(1-x)} \quad (18)$$

Where $\boldsymbol{b_\alpha^{Cu_2ZnSn(S_{1-x}Se_x)_4}}$ is the bowing parameter of $Cu_2ZnSn(S_{1-x}Se_x)_4$ energy dependent constant.

Table 5. Absorption coefficient constant α_0 of Cu_2ZnSnS_4 and $Cu_2ZnSnSe_4$ with bowing parameter b_α of $Cu_2ZnSn(S_{1-x}Se_x)_4$ absorption coefficient.

	Cu_2ZnSnS_4	$Cu_2ZnSnSe_4$
$\alpha_0 \times 10^4$(eV.cm^{-1})	15.274[a]	31.549[b]
	$Cu_2ZnSn(S_{1-x}Se_x)_4$ [22]	
$b_\alpha \times 10^4$(eV.cm^{-1})	2.471	

a and b are the values of the absorption coefficient constant α_0 of Cu_2ZnSnS_4 and $Cu_2ZnSnSe_4$, respectively, which are calculated from reference [11].

Furthermore, the effective state densities in the conduction band N_c and in the valence band N_v of $Cu_2ZnSn(S_{1-x}Se_x)_4$ can be calculated by Vegard's law:

$$N_c^{Cu_2ZnSn(S_{1-x}Se_x)_4}(x) = N_c^{Cu_2ZnSnS_4}(1-x) + N_c^{Cu_2ZnSnSe_4}x \quad (19)$$

$$N_v^{Cu_2ZnSn(S_{1-x}Se_x)_4}(x) = N_v^{Cu_2ZnSnS_4}(1-x) + N_v^{Cu_2ZnSnSe_4}x \quad (20)$$

Where $N_c^{Cu_2ZnSnS_4}$ and $N_c^{Cu_2ZnSnSe_4}$ are the effective state densities in the conduction band of Cu_2ZnSnS_4 and $Cu_2ZnSnSe_4$, respectively, $N_v^{Cu_2ZnSnS_4}$ and $N_v^{Cu_2ZnSnSe_4}$ their respective effective state densities in the valence band.

The effective state densities in the conduction band N_c and in the valence band N_v depend on temperature according to the following relations:

$$N_c = 2\left(\frac{2\pi m_e^* k_B T}{h^2}\right)^{\frac{3}{2}} \quad (21)$$

$$N_v = 2\left(\frac{2\pi m_h^* k_B T}{h^2}\right)^{3/2} \quad (22)$$

Where m_e^* et m_h^* are the effective mass of electrons in the conduction band and the effective mass of holes in the valence band, respectively, k_B is the Boltzmann's constant, T is the temperature in Kelvin and h is the Planck's constant ($h = 4.136\times10^{-15}$ eV.Hz^{-1}).

Table 6. Effective mass of electrons in the conduction band m_e^* and effective mass of holes in the valence band m_h^* of Cu_2ZnSnS_4 and $Cu_2ZnSnSe_4$. All numerical values are in units of free electron mass m_0 with $m_0 = 9.109\times10^{-31}$ Kg or $m_0 = 0.511$ MeV.c^{-2}.

	Cu_2ZnSnS_4 [28]	$Cu_2ZnSnSe_4$ [28]
m_e^*(MeV.c^{-2})	0.186 m_0	0.092 m_0
m_h^*(MeV.c^{-2})	0.454 m_0	0.203 m_0

3. Results and discussion

The effect of x composition on material stability was simulated and optimized at room temperature (Fig.2). Increasing the x composition causes an instability in $Cu_2ZnSn(S_{1-x}Se_x)_4$ /Cu_2NiGeS_4 structure. We note that the strain between the two materials is compressive i.e., ε is negative ($a_{CNGS}<a_{CZTSSe}$). Then an increase in x composition between 0 and 1 causes a significant increase in strain on the growth plane from 1.87 to 6.87% and from 2.05 to 6.96%, also along the growth direction from 2.68 to 7.40% and from 2.80 to 7.69% for kesterite and stannite structures, respectively. For example for x=0.10 the deformation between the two materials proposed are equal $\varepsilon_{xx(Kesterite)}$=2.39%, $\varepsilon_{xx(Stannite)}$=2.56% and $\varepsilon_{zz(Kesterite)}$=3.17%, $\varepsilon_{zz(Stannite)}$=3.31%. This simulation allows us to choose the most stable structure by optimizing the composition x

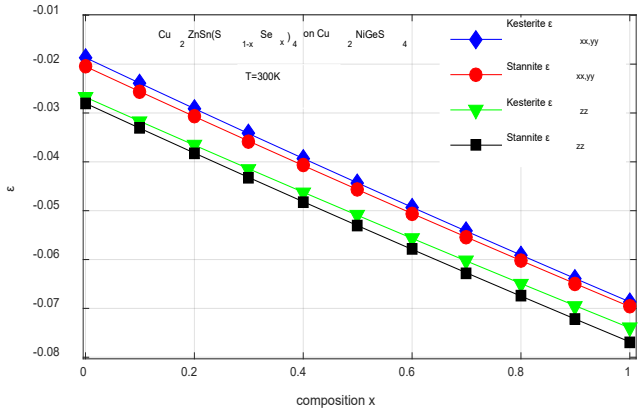

Fig.2. Lattice mismatch: Strained $Cu_2ZnSn(S_{1-x}Se_x)_4$ on Cu_2NiGeS_4 substrate as a function of Se content.

In Fig. 3 the x composition effect on the critical thickness of the $Cu_2ZnSn(S_{1-x}Se_x)_4$ and Cu_2NiGeS_4 structures has been simulated and analyzed.

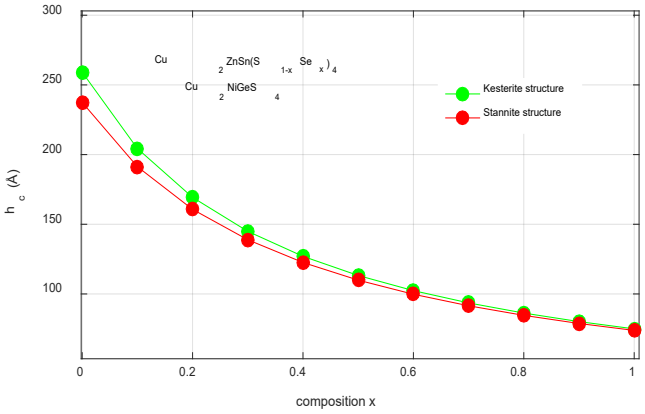

Fig.3. Critical thickness of $Cu_2ZnSn(S_{1-x}Se_x)_4$ as a function of Se content (Strained $Cu_2ZnSn(S_{1-x}Se_x)_4$ on Cu_2NiGeS_4 substr ate).

For the critical thickness, Fig.3 clearly shows that an increase in *Se* content markedly reduces this thickness for strained $Cu_2ZnSn(S_{1-x}Se_x)_4$ on Cu_2NiGeS_4 substrate. To obtain perfect growth of a pseudomorphic heteroepitaxy it is necessary that the thickness of $Cu_2ZnSn(S_{1-x}Se_x)_4$ must not exceed 25.91 and 23.75 nm for the kesterite and stannite structures, respectively, and for a very low Se composition. Beyond this thickness, the strain relaxes through

the formation of dislocations. According to Sellmeier equation (6), the dielectric constant of $Cu_2ZnSn(S_{1-x}Se_x)_4$ as a function of *Se* content and wavelength follows a nonlinearly increasing shape for near-infrared wavelengths, so it takes 131.522 as maximum value for *Se* rich structure and 8.822 as its minimum value for *Se* poor structure.

Fig.4. (a and b) show the effect of the incidence wavelength and the composition *x* on the permittivity of the proposed material at room temperature. In Fig.4.a, the effect of wavelength on the permittivity of two structures $CuZnSnS_4$ and $CuZnSnSe_4$ was shown. Increasing the wavelength causes a considerable decrease in the permittivity of two proposed structures. The wavelength and composition *x* influence on the permittivity of the $Cu_2ZnSn(S_{1-x}Se_x)$ structure was presented in Fig.4.b, when the wavelength and composition *x* vary from 0.8 to 1.2µm and 0 to 1, respectively, the permittivity of the material studied varies in the range from 8 to 18. This study allows us to optimize both the composition *x* and the permittivity of the alloy, then we will be able to choose them in order to create an efficient, stable and reliable structures.

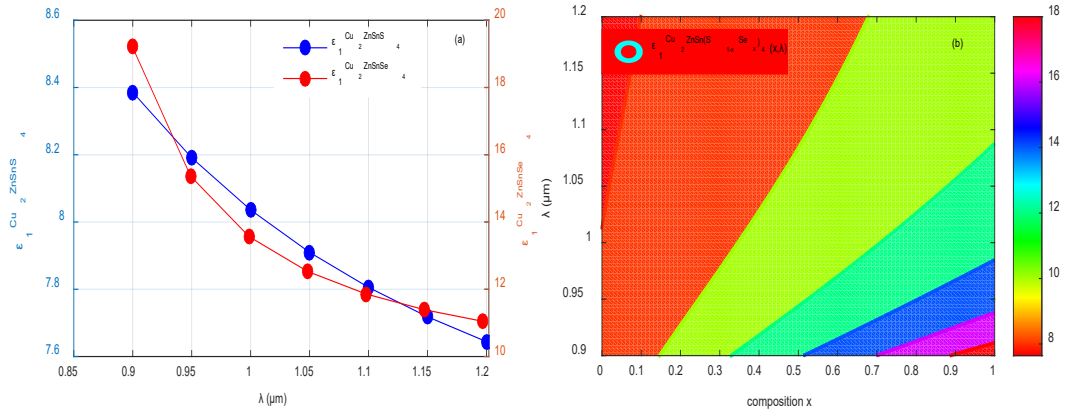

Fig. 4. Dielectric constant of: a) Cu_2ZnSnS_4 and $Cu_2ZnSnSe_4$ as a function of wavelength λ, b) $Cu_2ZnSn(S_{1-x}Se_x)_4$ as a function of wavelength λ and Se content.

Fig.5. (a and b) show the influence of the wavelength of incident photons and the composition *x* on the refractive index of the material studied at *T*=300K. In Fig.5.a. the variation of the refractive index as a function of wavelength of the tow structures $CuZnSnS_4$ and $CuZnSnSe_4$ has been simulated in 2D. We note that the refractive index varies from 3.2 to 4.4. In Fig.5.b. the wavelength and the composition *x* effect on the refractive index of the $Cu_2ZnSn(S_{1-x}Se_x)_4$ structure has been simulated in 3D.The refractive index *n* can be optimized by varying the composition*x* of the alloy. This study allows us to determine the optimal refractive index in order to choose the best structure. When we vary the wavelength λ and the composition *x* in the ranges from 0.82 to 0.9 µm and from 0 to1, respectively, the refractive index varies from 3 to 11. This optimization allows us to calculate the reflection and transmission coefficients, that is to say we will be able to study the reflection and transparency phenomena of the proposed material.

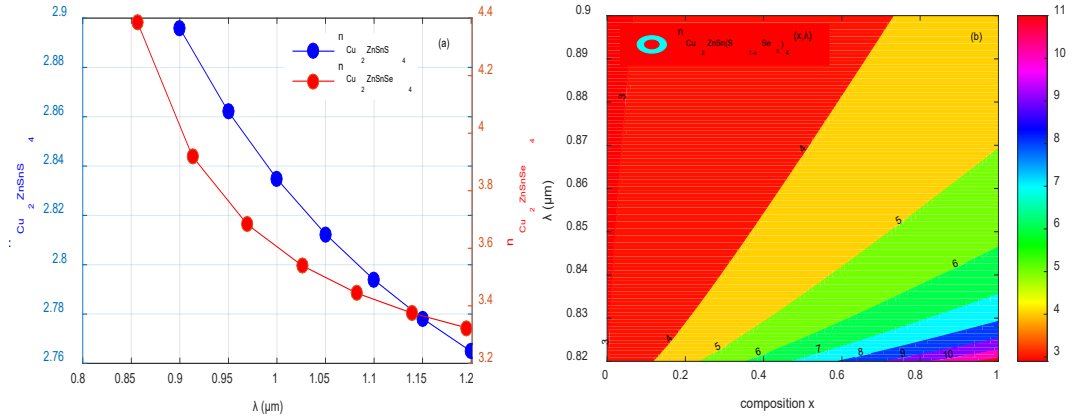

Fig.5. a) Refractive indices of Cu_2ZnSnS_4 and $Cu_2ZnSnSe_4$ as a function of wavelength λ, b) Refractive index of $Cu_2ZnSn(S_{1-x}Se_x)_4$ as a function of wavelength λ and Se content.

Fig.6. (a and b) show the influence of the incident photon wavelength and the composition *x* on the extinction coefficient *k* at *T*=300K. Fig.6.a. represents the evolution of extinction coefficients of Cu_2ZnSnS_4 and $Cu_2ZnSnSe_4$ as a function of wavelength in 2D. We note that the effect of wavelength on the extinction coefficient of $Cu_2ZnSnSe_4$ material is more important than that of $CuZn_2SnS_4$. When the wavelength is 0.700μm the extinction coefficients of Cu_2ZnSnS_4 and $Cu_2ZnSnSe_4$ reach 0.25 and 0.88, respectively. In Fig.6.b the effect of the wavelength of incident photon and the composition *x* of the alloy on the extinction coefficient was presented in 3D. When the wavelength varies from 0.1 to 0.8μm and the composition *x* of the alloy varies from 0 to 1, the extinction coefficient changes in the range from 0.1 to 0.9.

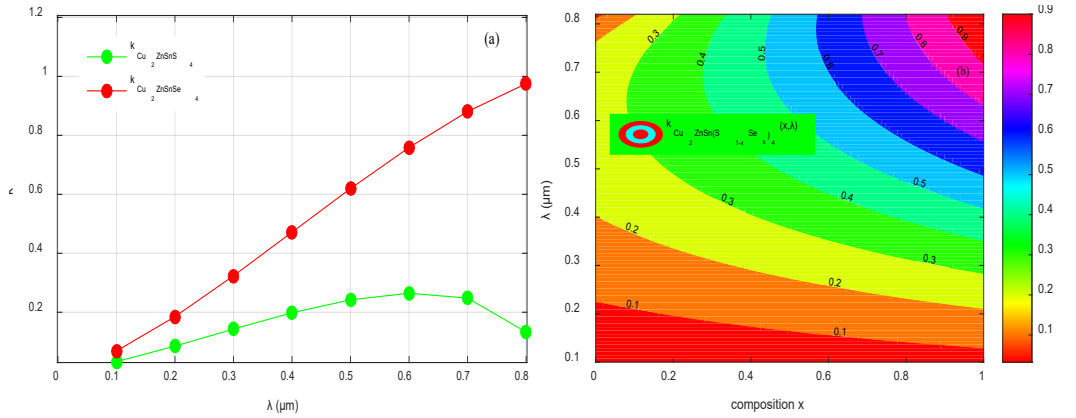

Fig.6. a) Extinction coefficients of Cu_2ZnSnS_4 and $Cu_2ZnSnSe_4$ as a function of wavelength λ, b) Extinction coefficient of $Cu_2ZnSn(S_{1-x}Se_x)_4$ as a function of wavelength λ and Se content.

On the other hand, the bandgap is remarkably influenced by *Se* content variations in $Cu_2ZnSn(S_{1-x}Se_x)_4$ kesterite structure, where it reaches its maximum value of 1.505 eV for *Se* poor structure, then it takes a decreasing pace until its minimum of 0.984 eV for *Se* rich structure (Fig.7.a). In Fig.7. b. the influence of temperature and composition *x* on the bandgap energy has been shown. We note that increasing the temperature and *Se* content causes a decrease in bandgap energy. This study allows us to optimize the bandgap energy in order to optimize the absorption coefficient of the proposed structure. For example, for *T*= 313K and a composition of 0.60 the bandgap energy equal to 1.186eV. Then, from Fig.7.b we will be able to detect the bandgap energy to choose an efficient and durable structure.

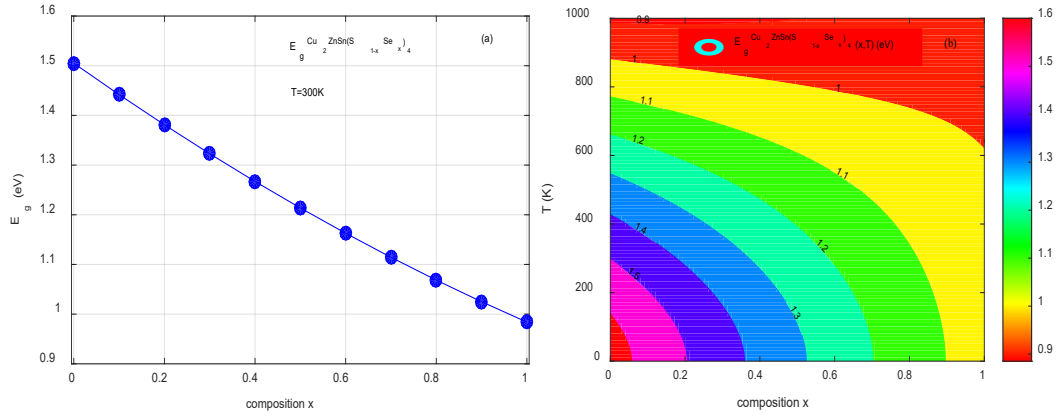

Fig .7. a) $Cu_2ZnSn(S_{1-x}Se_x)_4$ bandgap energy as a function of Se content, b) $Cu_2ZnSn(S_{1-x}Se_x)_4$ bandgap energy as a function of temperature and Se content.

In Fig.8. (a and b) we show the evolution of the variation of the absorption coefficient as a function of wavelength and the composition *x* at room temperature. Fig.8.a. shows the wavelength effect on the absorption coefficient of $CuZnSnS_4$ and $CuZnSnSe_4$ structures. We observe that the maximum absorption coefficient of the $CuZnSnS_4$ structure does not exceed $0.62\times10^5 cm^{-1}$ but the maximum absorption coefficient of the structure reaches $1.56\times10^5 cm^{-1}$. We have a gain of around $9.4\times10^4 cm^{-1}$. So, the $CuZnSnSe_4$ material is a better absorber compared to the $CuZnSnS_4$ material. The impact of wavelength and composition *x* on the absorption coefficient of the $Cu_2ZnSn(S_{1-x}Se_x)_4$ structure was simulated in Fig.8.b. We note that when the wavelength and the composition *x* change in the ranges from 0.1 to 0.8 µm and from 0 to 1, respectively, the absorption coefficient of $Cu_2ZnSn(S_{1-x}Se_x)_4$ structure varies from 0.2×10^5 to 1.4×10^5 cm^{-1}. This simulation allows us to optimize the absorption coefficient in order to choose the best structure for optoelectronic applications.

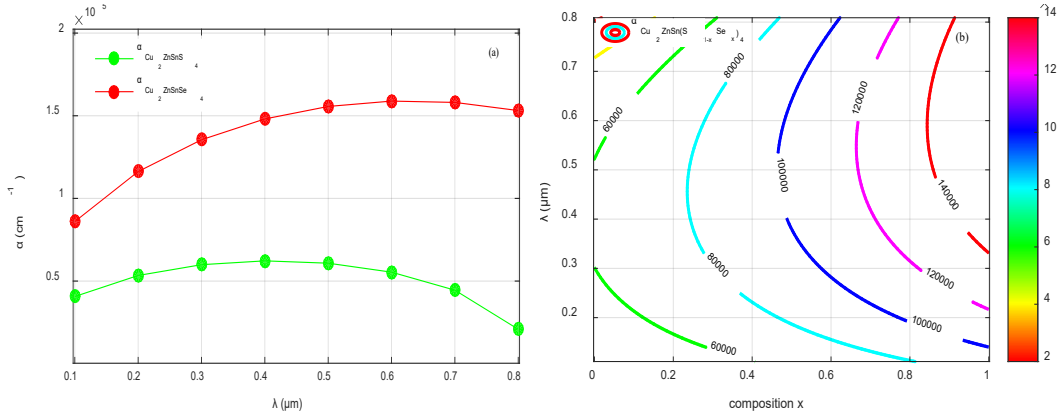

Fig. 8. a). Absorption coefficients of Cu_2ZnSnS_4 and $Cu_2ZnSnSe_4$ as a function of wavelength λ, b). Absorption coefficient of $Cu_2ZnSn(S_{1-x}Se_x)_4$ as a function of wavelength λ and Se content.

Fig.9.(a, b , c and d) show the evolution of the effective state densities in the conduction band N_c and in the valence band N_v, of which they are both strictly increasing as a function of temperature and slightly decreasing as a function of *Se* content.

Furthermore, Fig.9.a represents the variation of the effective state density of the electron and hole carriers of $CuZnSnS_4$ structure as a function of temperature. We observe that an increase in temperature induces a significant increase in both densities of states. Fig.9.b. illustrates the evolution of state density of the electron and hole carriers of $CuZnSnSe_4$ structure as a function of

temperature. We have the same phenomenon, that is to say an increase in temperature causes an increase in the density of state of the two electron-hole carriers but the effect is less compared to the first structure, we note that at room temperature, N_c and N_v take their values of 3.475×10^{18} and 1.325×10^{19} cm^{-3} for *Se* poor structure, and take their values of 1.209×10^{18} and 3.962×10^{18} cm^{-3} for *Se* rich structure, respectively. The temperature and the composition *x* effect on the density of state of electron of $Cu_2ZnSn(S_{1-x}Se_x)_4$ structure was studied (Fig.9.c). Also, the influence of temperature and composition x on the density of state of holes was taken into account (Fig.9.d). We note that this simulation allows us to optimize the densities of states of the electron-hole carriers and the mobility of the proposed structure.

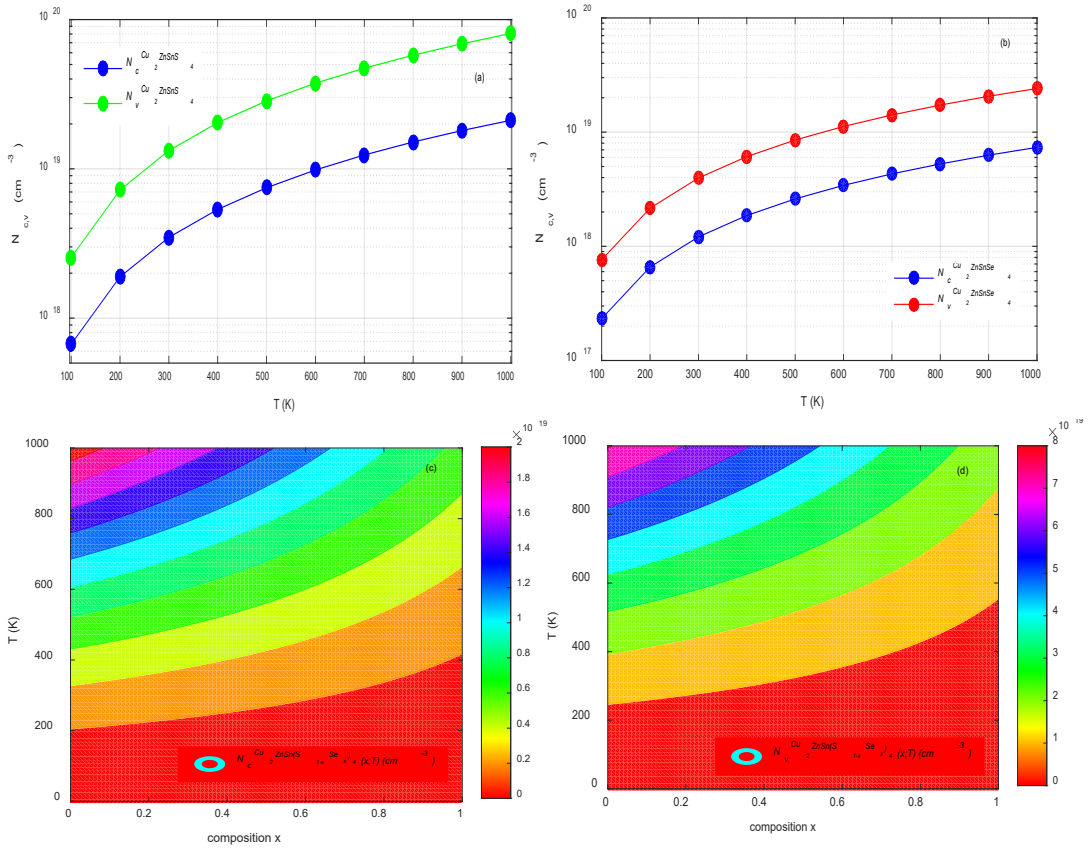

Fig .9. a) Effective state density in the conduction band N_c and in the valence band N_v of Cu_2ZnSnS_4 as a function of temperature, b) Effective state density in the conduction band N_c and in the valence band N_v of $Cu_2ZnSnSe_4$ as a function of temperature, c) Effective state density in the conduction band N_c of $Cu_2ZnSn(S_{1-x}Se_x)_4$ as a function of temperature and Se content and d) Effective state density in the valence band N_v of $Cu_2ZnSn(S_{1-x}Se_x)_4$ as a function of temperature and Se content.

4. Conclusion

After studying the structural, optical and electrical properties of $Cu_2ZnSn(S_{1-x}Se_x)_4$ semiconductor material, the analysis of the results obtained provided new insight into its use as an absorber layer in photovoltaic applications, in which, the *Se* content in $Cu_2ZnSn(S_{1-x}Se_x)_4$ semiconductor between 10 and 40%, is of primary importance in the characterization of solar cell. Consequently, the variations in $Cu_2ZnSn(S_{1-x}Se_x)_4$ optical parameters such as the refractive index, which is between 3.83 and 5.48 for near infrared wavelengths, as well as the extinction coefficient which varies in the range from 0.218 to 0.48 along the visible spectrum, moreover, the absorption coefficient which takes its values between 6.91×10^4 and 7.96×10^4 cm^{-1} also along the visible

spectrum. Furthermore, the bandgap energy which takes its values between 1.27 and 1.44 eV at room temperature, all these data are promising for good functional performance in photovoltaic applications. We can also conclude that $Cu_2ZnSn(S_{1-x}Se_x)_4$ alloys open a new way towards the use of new semiconductor materials which are more abundant in less expensive photovoltaic industry.

References

[1] W. Wang, M. T. Winkler, O. Gunawan, T. Gokmen, T. K. Todorov, Y. Zhu, D.B. Mitzi, AdvEnergy Mater, 4(7), 1(2013); https://doi.org/10.1002/aenm.201301465

[2] S. Chen, X. G. Gong, A. Walsh, S.H. Wei, American Physical Society, Physical Review B,79(16), 165211(2009); https://doi.org/10.1103/PhysRevB.79.165211

[3] B. Pamplin,JPhysChem, Solids, 25, 675(1964); https://doi.org/10.1016/0022-3697(64)90176-3

[4] J. Li, D. B. Mitzi, V.B. Shenoy,American Chemical Society,5(11), 8613 (2011); https://doi.org/10.1021/nn203230g

[5] X. Shi, Y. Wang, H. Yu, G. Wang, L. Huang, D. Pan, ACS Appl Mater Interfaces,12(37), 41590 (2020); https://doi.org/10.1021/acsami.0c12630

[6] J. He, L. Sun, S. Chen, Y. Chen, P. Yang, J. Chu,Journal of Alloys and Compounds, 511(1),129 (2012); https://doi.org/10.1016/j.jallcom.2011.08.099

[7] T. Tanaka, T. Nagatomo, D. Kawasaki, M. Nishio, Q. Guo, A. Wakahara, A. Yoshida, H. Ogawa,Journal of Physics and Chemistry of Solids,66(11), 1978 (2005); https://doi.org/10.1016/j.jpcs.2005.09.037

[8] S. Chen, X. G. Gong, A. Walsh, S.H. Wei,Appl Phys Lett,96(2), 021902 (2010); https://doi.org/10.1063/1.3275796

[9] J. Paier, R. Asahi, A. Nagoya, G. Kresse,Physical Review B,79(11), 115126 (2009); https://doi.org/10.1103/PhysRevB.79.115126

[10] M. Kumar, C. Persson, International Journal of Theoretical & Applied Sciences, 5(1), 1(2013).

[11] C. Persson, Journal of Applied Physics,107(5), 053710 (2010); https://doi.org/10.1063/1.3318468

[12] I.Vurgaftman, J.R. Meyer,Journal of Applied Physics,94(6), 3675 (2003); https://doi.org/10.1063/1.1600519

[13] G.E. Delgado, V. Sagredo,Revista Mexicana de Física,65(4), 355 (2019); https://doi.org/10.31349/RevMexFis.65.355

[14] A.Aissat, J.P. Vilcot, Optik,207, 163844 (2020); https://doi.org/10.1016/j.ijleo.2019.163844

[15]J.W. Matthews, A.E. Blakeslee,Journal of Crystal Growth, 27, 118 (1974); https://doi.org/10.1016/S0022-0248(74)80055-2

[16] M. León, S. Levcenko, R. Serna, G. Gurieva, A. Nateprov, J. M. Merino, E. J. Friedrich,U. Fillat, S. Schorr, E. Arushanov,Journal of Applied Physics,108(9), 093502 (2010); https://doi.org/10.1063/1.3500439

[17] S.G. Choi, H.Y. Zhao, C. Persson, C.L. Perkins, A.L. Donohue, B. To, A.G. Norman, J. Li and I.L. Repins, Journal of Applied Physics,111(3), 033506 (2012); https://doi.org/10.1063/1.3681814

[18] J. Li, H. Du, J. Yarbrough, A. Norman, K. Jones, G. Teeter, F. Lewis Terry, D. Levi,Optics Express,20(S2), 327 (2012); https://doi.org/10.1364/OE.20.00A327

[19] S. Adachi, Properties of Group-IV, III−V and II−VI Semiconductors, John Wiley & Sons, Chichester, 2-163 (2009).

[20] S. Adachi, Chapter 7: Physical Properties, Compiled Experimental Data. Copper Zinc Tin Sulfide-Based Thin-Film Solar Cells, John Wiley & Sons, 150-179 (2015); https://doi.org/10.1002/9781118437865.ch7

[21] Z.Y. Zhao, Q.L. Liu, X. Zhao, Journal of Alloys and Compounds, 618, 248(2015); https://doi.org/10.1016/j.jallcom.2014.08.213

[22] S. Tripathi, B. Kumar, D.K. Dwivedi, Journal of Materials Science: Materials in Electronics,31, 8308 (2020); https://doi.org/10.1007/s10854-020-03366-y

[23] S. Islam, M. Rahaman, M.A. Gafur, M.K. Hossain, F. Ahmed, M. Abul, Journal of Materials Science and Engineering,8(9-10),198 (2018)

[24] S. Schorr, R. Mainz, H.Mönig, I. Lauermann, M. Bär, Progress in Photovoltaics,20(5),557 (2012); https://doi.org/10.1002/pip.1256

[25] P.K.Sarswat, M.L. Free, Physica B, 407(1), 108 (2012); https://doi.org/10.1016/j.physb.2011.09.134

[26] M.V. Yakushev, I. Forbesc, A.V. Mudryi, M. Grossberge, J. Krustoke, N.S. Beattie, M. Moynihan, A. Rockett, R.W. Martina,Thin Solid Films, 582, 154 (2015); https://doi.org/10.1016/j.tsf.2014.09.010

[27] C.Stroth, M.H. Sayed, J.Neerken, U. Mikolajczak, G. Rey, J. Parisi and L.Gütay, AIP Advances,7(2), 025303 (2017); https://doi.org/10.1063/1.4976619

[28] B. Wang, H. Xiang, T. Nakayama, J. Zhou, B. Li, Physical Review B, 95(3),035201 (2017); https://doi.org/10.1103/PhysRevB.95.035201